

# Re-entrant waves and their elimination in a model of mammalian ventricular tissue<sup>★</sup>

V.N. Biktashev<sup>a,b</sup> and A.V. Holden<sup>b,1</sup>

<sup>a</sup> *Institute for Mathematical Problems in Biology, Pushchino, Moscow Region, 142292, Russia*

<sup>b</sup> *Department of Physiology, University of Leeds, Leeds LS2 9JT, UK*

The vulnerability to re-entrant wave propagation in 1-, 2- and 3-D models of normal mammalian ventricular tissue, its characteristics (period, meander and stability), the effects of rotational transmural anisotropy, and the control of re-entrant waves by small amplitude perturbations and large amplitude defibrillating shocks are investigated theoretically and numerically for models based on high order, stiff biophysically derived excitation equations.

---

<sup>★</sup> Submitted to *Chaos*

<sup>1</sup> Author to whom correspondence should be addressed

The re-entrant ventricular arrhythmias of monomorphic ventricular tachycardia and fibrillation are produced by abnormal spatio-temporal patterns of propagation in the ventricular myocardium. These behaviours can be described by solutions of reaction-diffusion equation excitable medium models, in which the reaction terms come from the results of voltage clamp analyses of cell excitation processes, — membrane currents and pumps, intra- and extracellular ion accumulation and intracellular sequestration processes, and the diffusion coefficient tensor is obtained from the propagation velocity and scaled muscle fibre orientation. Numerical solution of such biophysical detailed models allow the screening putative antiarrhythmic agents, by computing their effects on vulnerability to re-entry, and the specification of means of pharmacologically modifying meander, to enhance the self-termination of re-entry. Quantitative aspects of defibrillation, by extinguishing propagating waves of excitation by a single shock, or by resonant drift induced by appropriately timed small amplitude, can be computed.

## 1 Introduction

Some cardiac arrhythmias are due to re-entrant propagation, in which the same wavefront repeatedly re-invades the same piece of tissue after propagating around an anatomical or functional block. Monomorphic ventricular tachycardia is probably produced by simple re-entry [1,2] and the order remaining in ventricular fibrillation [3,4] may be due to re-entrant waves. The relatively thick wall of the ventricle means that propagation in ventricular muscle could be a predominantly three-dimensional phenomenon that occurs in an anisotropic and heterogeneous tissue, or could be explained by two-dimensional phenomena that result from the excitation properties rather than heterogeneity and anisotropy. In this paper we obtain the characteristics of propagation in one-, and two-dimensional, homogeneous model of ventricular tissue, and use these to account for the linear regions of unidirectional conduction blocks seen in mapping studies [5,6], to interpret the changes in conduction velocity of a re-entrant wave around an extended obstacle [7], to explain why it is difficult to establish re-entrant propagation in the healthy ventricle, and to quantitatively assess single shock and resonant drift methods of eliminating re-entry from ventricular tissue.

There are a number of published and available models for ventricular excitation that summarise the results of voltage clamp experiments on ventricular tissue and cells — these include the Beeler-Reuter model [8], the Oxsoft guinea pig ventricular cell model specified in Noble *et al.*[9,10], the Nordin [11] model and the phase 2 Luo-Rudy [12] model and its recent modification [13]. None

of these models are definitive, they all represent steps in an on-going process of modelling the behaviour of different types of ventricular cells by a description of membrane currents and pumps, and intracellular ion binding and concentration changes [14].

In this paper we use equations of the Oxsoft guinea pig ventricle model [9,10], later referred to as OGPV. These equations provide a convenient starting point, and can be modified to simulate *e.g.* the effects of epicardial to endocardial changes in ventricular action potential described by Antzelevitch [15,16], long QT syndrome [17], and ischaemia - see Boyett *et al.*[18]. We construct an excitable medium model for mammalian ventricular tissue by incorporating ordinary differential equations for ventricular cell excitability into a reaction-diffusion system of differential equations with the voltage diffusion coefficient selected to give an appropriate conduction velocity. For a homogeneous two dimensional medium, the effects of homogeneous anisotropy can be included by a simple rescaling of coordinates.

## 2 The numerical model

The Oxsoft equations [9] summarise the results of extensive voltage clamp and ion flux investigations on mammalian ventricular tissue and cells, and provide a model for the membrane currents resulting from voltage-dependent gated, and leakage, conductances; active transmembrane exchanges; and intracellular ion concentration changes, and  $\text{Ca}^{2+}$  release and sequestration from the sarcoplasmic reticulum in a single ventricular myocyte. In this paper, we use the model of guinea pig ventricular cell from the Oxsoft family, the basic ideas of which can be found in [10], the OGPV model.

For a single isopotential cell the model is in the form of a system of ordinary differential equations, which can be shortly written in the form

$$\begin{aligned} C\partial_t V &= f(V, \mathbf{u}, \mathbf{w}), \\ \partial_t \mathbf{u} &= \mathbf{g}(V, \mathbf{u}, \mathbf{w}), \\ \partial_t \mathbf{w} &= \mathbf{h}(V, \mathbf{u}, \mathbf{w}), \end{aligned} \tag{1}$$

where  $V = V(t)$  is the transmembrane voltage,  $C$  is cell capacitance,  $f$  is transmembrane current density, vector  $\mathbf{u} = \mathbf{u}(t)$  describes the fast gating variables, and vector  $\mathbf{w} = \mathbf{w}(t)$  comprises slow gating variables and intra- and extra-cellular ionic concentrations, and  $\mathbf{g}$  and  $\mathbf{h}$  describe their kinetics. Action potential solutions of this model and their rate dependence are illustrated in Fig. 1(a-c).

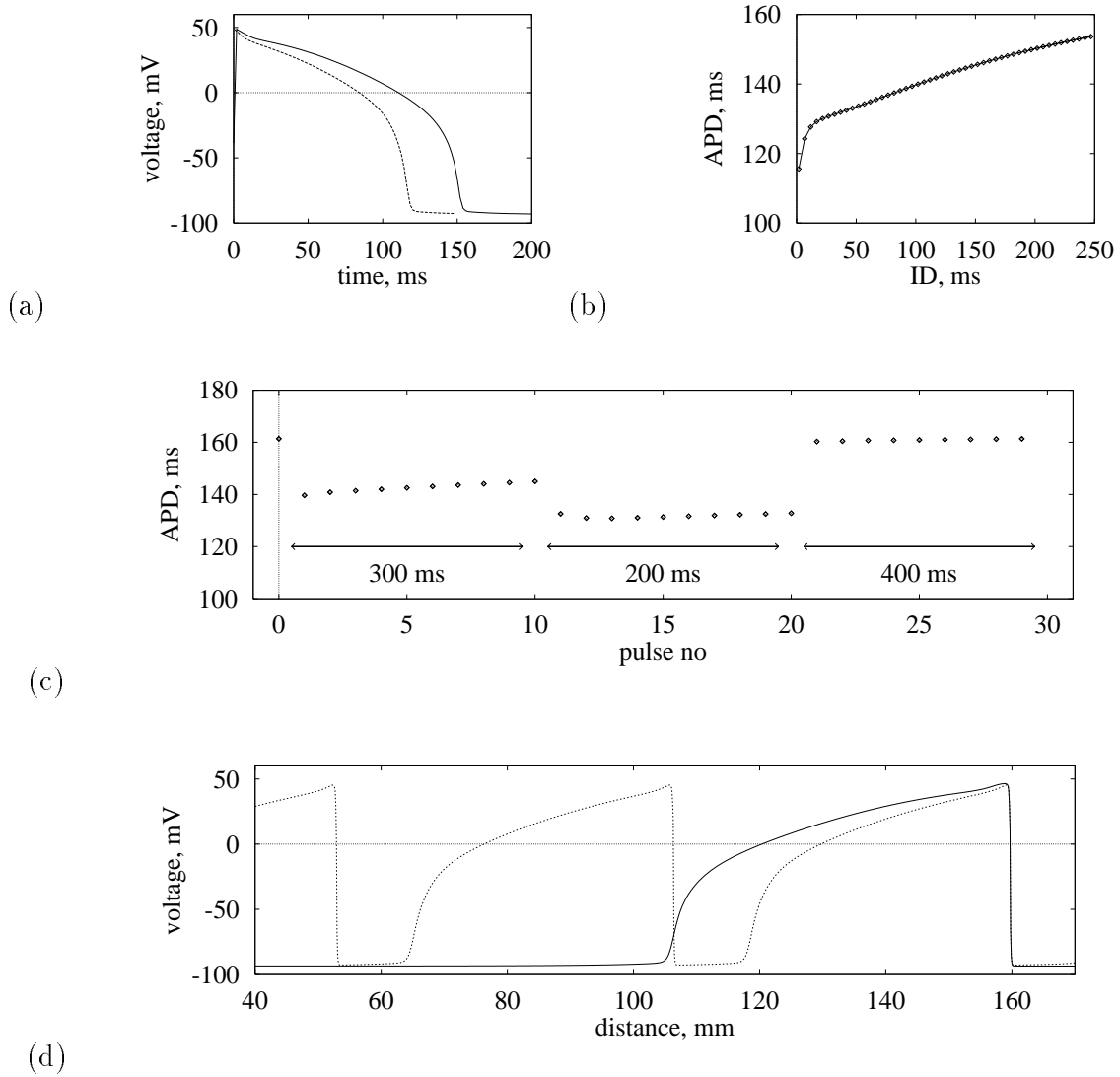


Fig. 1. The OGPV model. (a) Action potential for normal (400 ms, solid line) and high (150 ms, dashed line) pacing rates. (b) Restitution curve, action potential duration vs diastolic interval, measured at 95% (-86 mV). (c) Variations of APD during pacing with changing period (shown by arrows). (d) Voltage profiles of propagating pulses, at normal (400 ms, solid line) and high (150 ms, dashed line) pacing rates.

This model was incorporated into a partial differential equation model for an excitable medium in the plane  $(x, y)$

$$\begin{aligned}
 \partial_t V &= C^{-1} f(V, \mathbf{u}, \mathbf{w}) + D \nabla^2 V + F(x, y, t) \\
 \partial_t \mathbf{u} &= \mathbf{g}(V, \mathbf{u}, \mathbf{w}), \\
 \partial_t \mathbf{w} &= \mathbf{h}(V, \mathbf{u}, \mathbf{w}),
 \end{aligned} \tag{2}$$

where  $D$  is the diffusion coefficient for  $V$ ,  $\nabla^2$  is the Laplacian operator  $(\partial_x^2 + \partial_y^2)$  and  $F(x, y, t)$  is a time and space dependent forcing that models external

electric current applied to the tissue; as written in (2) it has the dimensionality of voltage over time, and can be rescaled to current units *via* the value of  $C = 0.2$  nF. The diffusion coefficient  $D = 31.25$  mm<sup>2</sup>s<sup>-1</sup> was chosen to give a conduction velocity for a solitary plane wave along one of the coordinate axes of 400 mm/s. Canine ventricular conduction velocities range from 140–250 (transverse) to 500–800 (longitudinal) mm/s [19].

Calculations were performed using the explicit Euler method (except ‘m’ gating variable which was calculated implicitly) with five-node approximation of the Laplacian on a rectangular grid of  $200 \times 200$  to  $300 \times 300$  nodes with a time step of 0.01 to 0.05 ms and a space step of 0.1 mm, with impermeable boundaries

$$\partial V / \partial x \Big|_{x=x_{\min}, x_{\max}} = \partial V / \partial y \Big|_{y=y_{\min}, y_{\max}} = 0. \quad (3)$$

Spiral waves were initiated in one of three ways, by a cut wavefront, twin pulse protocol, or a phase distribution method. A plane wave was initiated at one edge of the medium by a 2 ms duration stimulation of a strip 1.3 mm wide, by a current  $F(x, y, t)$  that gave a  $dV/dt$  of 50 mV/ms (10 nA/cell) and the excitation allowed to propagate to the centre of the medium. The wavefront was then cut, and all the variables on one side of the cut reset to their equilibrium values. This numerically convenient but artificial method allows spirals to be initiated in a  $20 \times 20$  mm medium. The twin pulse protocol [20] requires a larger ( $30 \times 30$  mm) medium, in which a plane wave is initiated at the lower border by 10 ms stimulation of 50 mV/ms (10 nA/cell) of a two mm strip, and 180 ms later (after the wavefront has propagated through the medium, establishing a gradient in refractoriness) the second stimulus is applied: a 4 ms stimulation of 40 mV/ms (8 nA/cell) over the left  $30 \times 25$  mm area of the medium.

The phase distribution method used one-dimensional calculations to record values of all dynamical variables in a plane periodic wave of a high frequency, thus expressing all the 17 variables as functions of single scalar variable, the phase. To create initial conditions, a distribution of the phase over the plane, corresponding to an Archimedean spiral with an appropriate wavelength, has been used to specify the distribution of the dynamic variables *via* these functions. This highly artificial method is convenient to produce spiral wave at a prescribed location. However, it still requires large enough medium to initiate (we used  $20 \times 20$  mm), as the larger core in the first revolutions of the spiral is determined not only by the initiation procedure, but by internal properties of the medium.

### 3 One dimensional vulnerability

The reaction-diffusion equation (2) in one dimension has a spatially uniform solution, corresponding to resting tissue, and can support solitary wave and wave train solutions. The solitary travelling wave solution propagates at a velocity proportional to the root of the diffusion coefficient, and so the diffusion coefficient can be chosen to give appropriate length and velocity scaling. Fig. 1(*d*) illustrates travelling wave train solutions; at the higher rate the action potential duration is shortened, and the action potential velocity is reduced, and the spatial extent (the "wavelength", say measured at 95% repolarisation) is shortened. Thus although there may not be enough room in the heart for more than one action potential at low rates, as rate is increased the shorter wavelength may allow more than one action potential.

Two travelling wave solutions meeting head on collide and annihilate each other; this destructive interference results from the refractory period of the travelling waves. Supra-threshold stimulation at a point in a uniformly resting one-dimensional model produces a pair of travelling wave solutions that propagate away from the initiation site. The initiation of a single solitary wave in a one-dimensional ring provides a computationally simple model for re-entry; such unidirectional propagation can only be produced in a homogeneous one-dimensional medium if the symmetry is broken, say by a preceding action potential. Fig. 2(*a-c*) illustrate the responses of a one dimensional ventricular tissue model to stimulation at different times in the wake of an action potential. The vulnerable window is the period after a preceding action potential during which a unidirectional wave in a one dimensional medium can be initiated; stimulation during the vulnerable period in the wake of a plane wave in a two-dimensional medium would initiate a pair of spiral waves. Thus the test pulse in Fig. 2(*b*) falls into the vulnerable window.

Starmer *et al.* [21] have characterised the vulnerable window for Beeler-Ruter and FitzHugh-Nagumo models. The numerical results of Fig. 2(*d*) show the expected increase in the vulnerable window with stimulus intensity and with the length of the stimulated tissue (the electrode size). If the effects of pharmacological agents or pathological processes (ischaemia, acidosis) can be expressed as changes in the excitation system (1) then repeating the computations of Fig. 2 provides a means of quantifying the pro- or anti-arrhythmic effects of these changes.

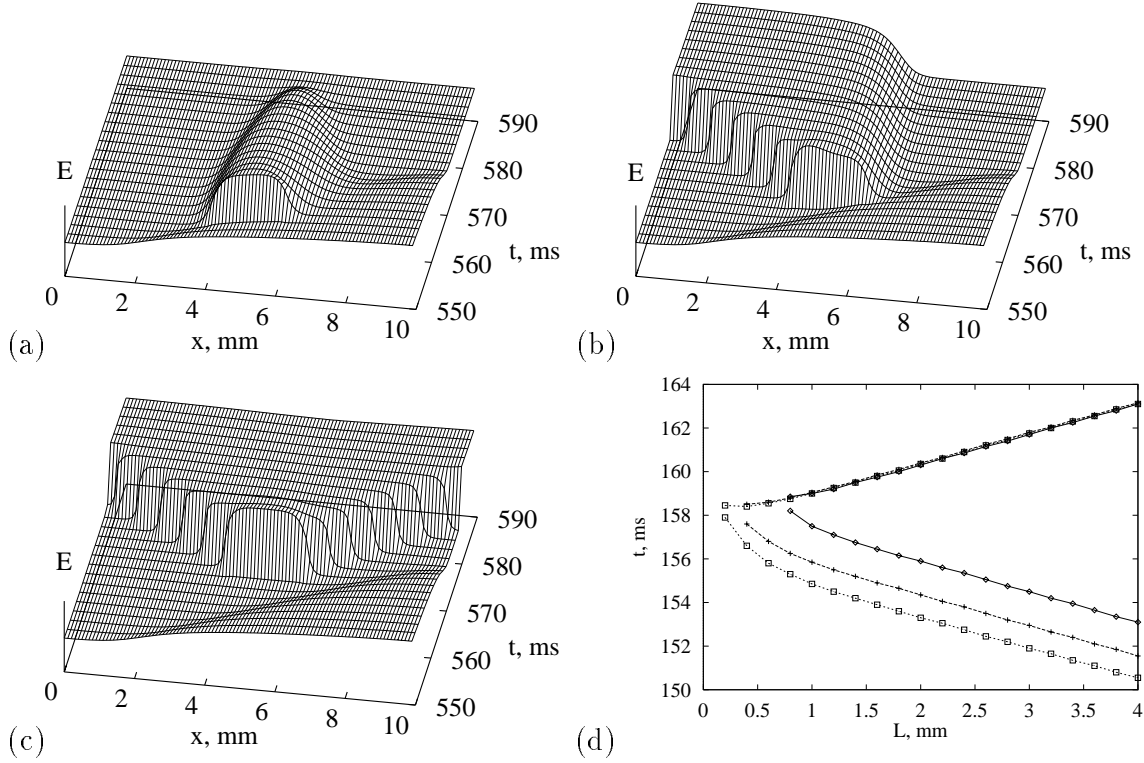


Fig. 2. 1-D vulnerability in the OGPV model. Two conditioning pulses with the interval of 400 ms passed through the medium rightwards, then the test pulse was delivered in the wake of the last conditioning wave. (a)–(c) shows no, uni- and bi-directional responses to the test stimuli of the same amplitude  $2 \text{ ms} \times 50 \text{ mV/ms}$  of the same 2 mm piece of the medium, but delivered at different time moments. (d) shows vulnerable window (ordinate, earliest and latest time delay after the start of the last conditioning wave) for unidirectional response, as function of electrode size (abscissa) and stimulus amplitude (shown as label on each line, mV/ms), with center of the stimulated region fixed.

#### 4 Two dimensional phenomena

Figure 3 illustrates a spiral wave solution of the model, as the spatial distribution of the membrane potential  $V$ , at an instant 2.67 s after the spiral wave was initiated by cutting a broken plane wave half way up the medium. The wavefront of the action potential is the sharp transition between light and dark shade, and far from the tip of the spiral the wavelength of the spiral (the distance between successive wavefronts) is about 40 mm. The spiral rotated with an initial period of approximately 170 ms, and over the first 1 s the period decreased to 100–110 ms. The tip of the spiral may be defined by the intersection of two isolines; we define the tip by the intersection of the  $V = -10 \text{ mV}$  and the  $f = 0.5$  isolines, where  $f$  is the  $\text{Ca}^{2+}$  (slow inward) current inactivation gating variable. The trajectory of the tip of the spiral is not stationary, but meanders, and its motion is nonuniform, moving by a jump-like alternation

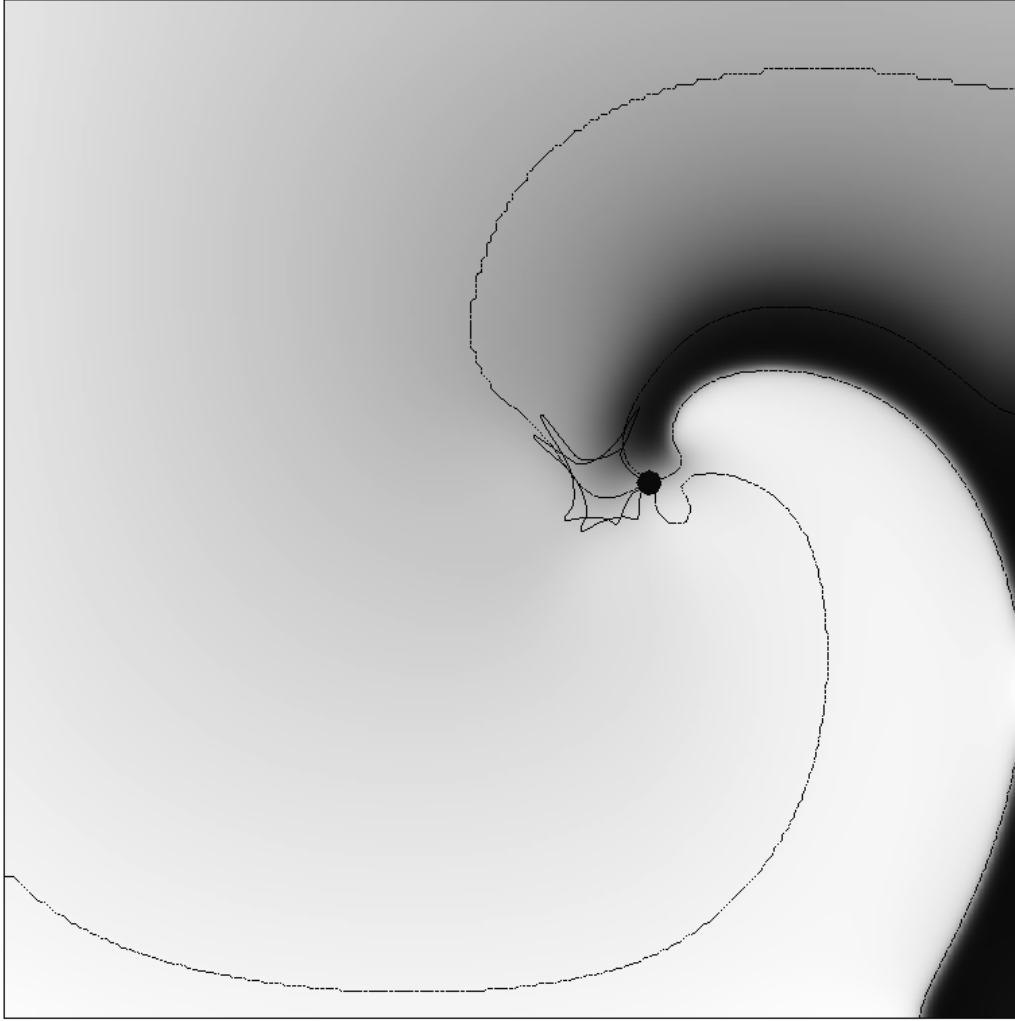


Fig. 3. Snapshot of a spiral wave in the OGPV model. Grayscale shading codes the transmembrane voltage, white is depolarisation and dark is repolarisation. Shown are two isolines, one of the voltage and the other of the  $I_{s_i}$  inactivation gate 'f'. Crossing of the two isolines is the instant position of the spiral tip shown by black circle. The flower-like line is trajectory of the tip in the last two rotations.

between fast and very slow phases, with about 5 jumps per full rotation. This motion resembles an irregular, nearly biperiodic process, with the ratio of the two periods close to 1:5.

The rotation of the spiral wave can be monitored by following an isoline on the wavefront, and the trajectory of the tip of the spiral, as illustrated in Fig. 3. The area enclosed by the tip trajectory is analogous to the core of a rigidly rotating spiral, and is not invaded by the action potential. Characteristics of the  $V(t)$  observed at different sites in the medium during the evolution of a rotating spiral wave are:

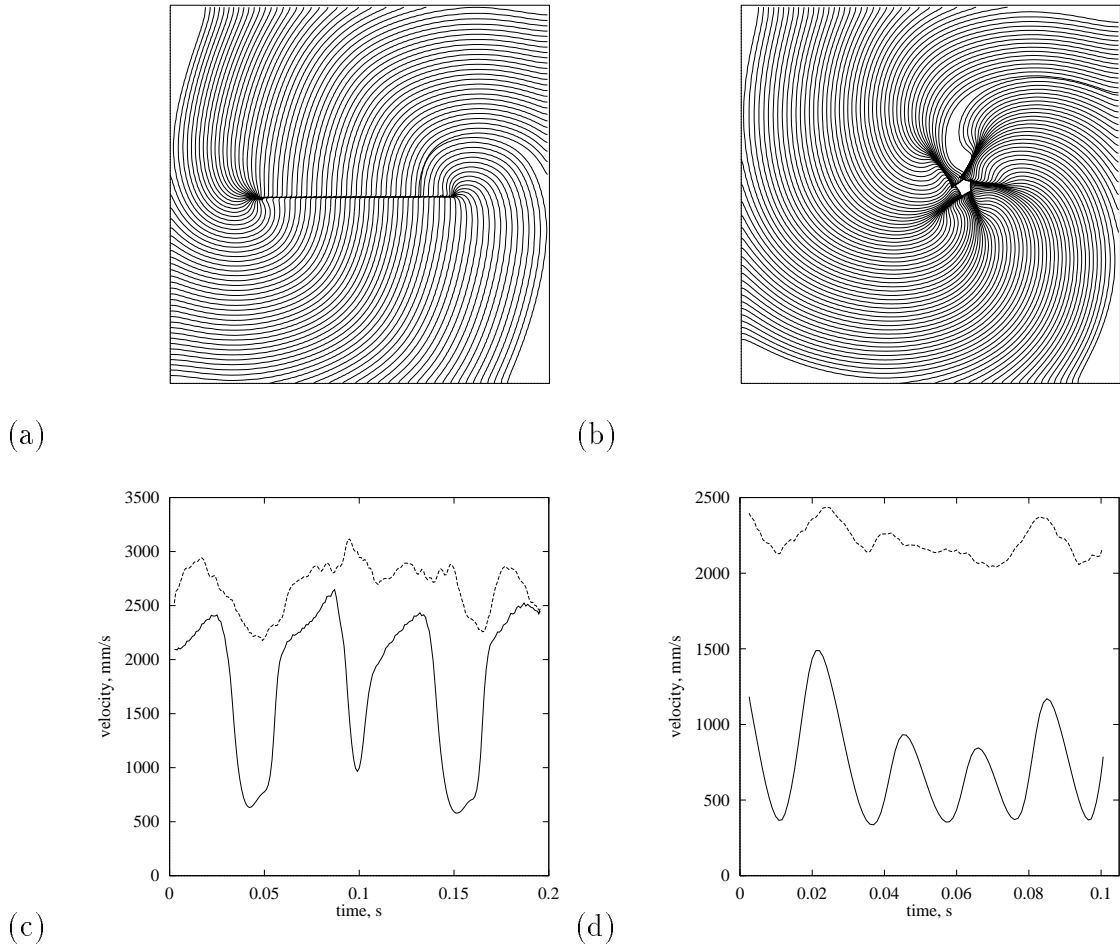


Fig. 4. Nonuniformity of propagation velocity around a hole (left column) and in a spiral wave (right column). Top: isochronal map of one rotation with 1 ms step between isochrones. Bottom: variation of propagation velocity with time during the rotation; solid line at the distance 0.5 mm and the dashed line at 5 mm from the tip along the isochrones.

- only the first action potential, produced by activity invading a resting medium, has the fast depolarisation and overshoot that are characteristic of solitary membrane action potential solutions of (1),
- far from the tip of the spiral wave, the repetitive action potentials are faster and larger than closer to the tip,
- close to the tip the repetitive activity is not only are smaller in amplitude, and have reduced  $\partial V/\partial t_{\max}$ , but appear more as complicated oscillations than action potentials.

These different behaviours occur in an initially homogeneous medium, in which re-entry has established a functional inhomogeneity, and are similar to the behaviours of all functional re-entry waves in excitable medium, and to waves in excitable media rotating around a small obstacle.

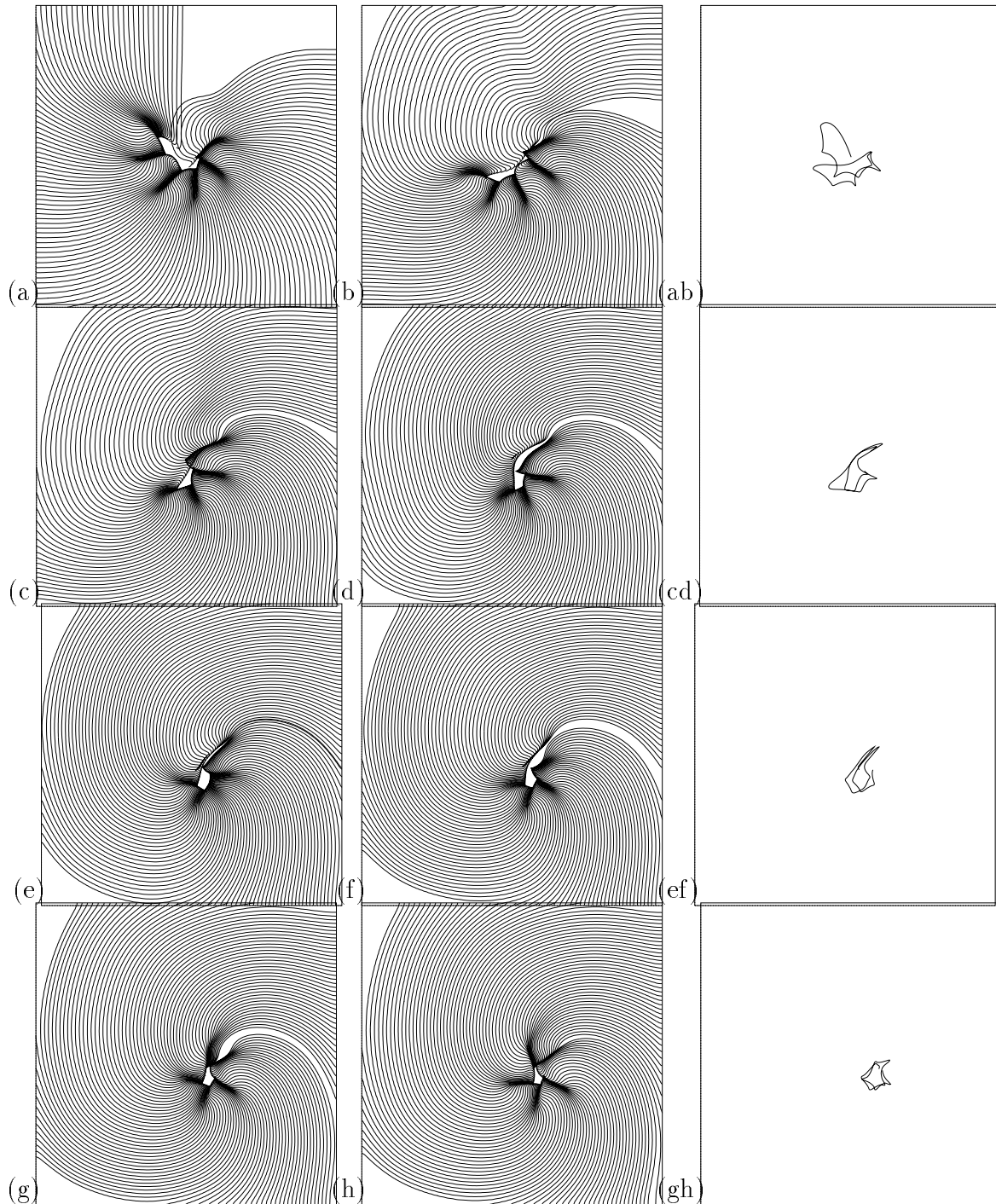


Fig. 5. Development and ageing of spiral wave after initiation by phase distribution initial conditions. Two left columns show successive 1-ms isochronal maps; the right columns shows corresponding pieces of tip trajectory.

Within the functional block or core the membrane potential remains between -45 and -5 mV; this persistent depolarisation means the inward  $i_{Na}$  is inactivated, blocking propagation into the core. The principal currents ( $i_{Na}$ ,  $i_{Ca}$ ,  $i_{K1}$ ,  $i_f$ ) far from, and within the core are examined in [31].

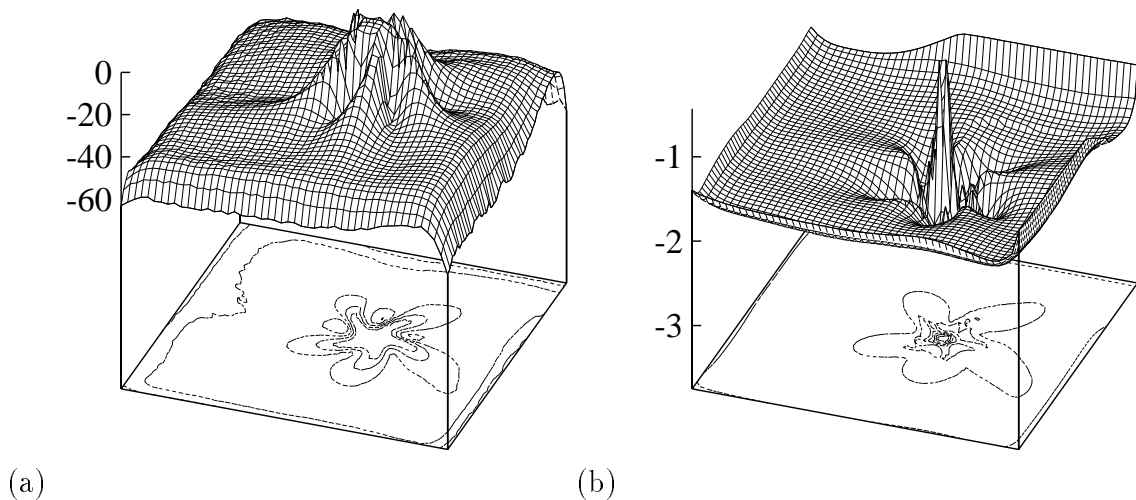


Fig. 6. The role of the two major excitatory currents,  $I_{Na}$  (left) and  $I_{si}$  (right), in forming the shape of the core. Shown are the distribution of the minimal (i.e. maximal in the absolute value) currents throughout the preparation during 110 ms, i.e. slightly longer than one rotation of the spiral wave, same as shown in fig. 4. Vertical axes show values of the currents in nA per cell.

After an initial transient, the spiral is rotating around a compact core contained within a few mm square. The multi-lobed pattern of the trajectory of the tip illustrated in Fig. 3 takes time to develop, and itself continues to develop with time. This time evolution, or "ageing" is described in [31] and has been ascribed to the slow changes in intracellular concentrations that occur in the Oxsoft models.

A different approach to examining this ageing appears by plotting the voltage isochrones every ms, as in Fig. 5. Here the spiral was initiated from initial conditions specified by the phase distribution method, to prevent any extended structures being produced by the method of initiation of the spiral. Close to the tip of the spiral the distance between the isochrones changes, and so the local wavefront velocity is changing, with slow velocities occurring at the sharp turns of the tip. Bunching of isochronal lines is interpreted as an arc of conduction block in clinical cardiac mapping studies. The spirals initiated from a broken wave and by the cross field technique have more pronounced transients, and their tip evolution is described in [31]. The pattern of the tip motion and the associated velocity of the wavefront near the tip is continually changing, and the early tip trajectory resembles the linear extended tip trajectories seen in the Beeler-Reuter model [22]. However, the slowing down occurs along the linear segments of the trajectory, as well as at the sharp corners.

Girouard *et al.* have studied propagation of re-entrant waves around a laser induced linear obstacle in the guinea-pig heart. Fig. 4 compares propagation around a thin linear obstacle (left) with propagation around a functional block.

The isochronal maps show the slowed propagation associated with the sharp turns, and the local normal wavefront propagation velocity. For the obstacle, the slowing down is confined to the ends of the obstacle, where the curvature is large, and is consistent with the observations of Girouard *et al.* For the functional block there is not a clear connection between the curvature and the velocity.

We believe that around the obstacle, the slowing down is predominantly due to curvature effects, while for the functional block the dominant effect is the propagation of the wavefront into a region of refractory tissue. Although the wavefront, driven only by  $\text{Na}^+$  current cannot propagate deep into a region where this current is inactivated,  $\text{Ca}^{2+}$  current can carry the wavefront into refractory region. This is analogous to the interpretation of the onset of irregularity in re-entry in the Beeler-Reuter model as due to interactions between  $\text{Na}^+$  and  $\text{Ca}^{2+}$  activation fronts [23].

We can illustrate this by blocking  $\text{Ca}^{2+}$ -conductance, which leaves a simple rigidly rotating spiral, or by visualising the maximum currents during one rotation. Fig. 6 shows the maximal magnitude of the principal depolarising currents,  $I_{\text{Na}}$  and  $I_{\text{si}}$  during just over one rotation, the same computation as in Fig. 5. While sodium current shows the five-petal star shape of the block (the region where it was nearly zero throughout the rotation), the calcium current has small circular block and only slightly modulated around. Thus, the meandering petals can be interpreted as loci where fast sodium waves died out and propagation was supported by slow calcium waves. The five-lobed pattern is not an attractor, as its shape is continually and slowly changing. However it is persistent for long enough to be considered the state of the spiral wave we would seek to eliminate in section 5; it is important to note that its behaviour and evolution can be understood in terms of the dynamic balancing between the fast and slow depolarising currents, rather than simple curvature and electrotonic loading effects.

## 5 Defibrillation

### 5.1 Resonant drift

The tip of the spiral wave solutions presented in Fig. 3–6 moves irregularly in a complicated trajectory, but does not move out of the medium: if the medium is large enough to contain the early transient motion around an almost linear core then the spiral wave remains in the medium.

Small amplitude, spatially uniform repetitive stimulation can be used to pro-

duce directed movement of a rigidly rotating spiral wave, if the period of stimulation is equal to the period of the spiral wave rotation (resonant drift). If the stimulation period is close but not equal to the rotation period of the spiral a circular drift is obtained [24,30]. If the stimulation period is fixed, this drift is strongly influenced by medium inhomogeneities [25]. Such a drift has been observed in reaction-diffusion model of rabbit atrium based on Earm-Hilgemann-Noble kinetics [36]. In the OGPV model, even in the absence of inhomogeneities, the instantaneous frequency of the spiral is always changing, because of the meander and the slow change of the spiral wave period due to ageing and so a pure resonant drift is not observed at any constant frequency. A typical trajectory, produced by constant frequency perturbation of a meandering OGPV spiral, is shown in Fig. 7.

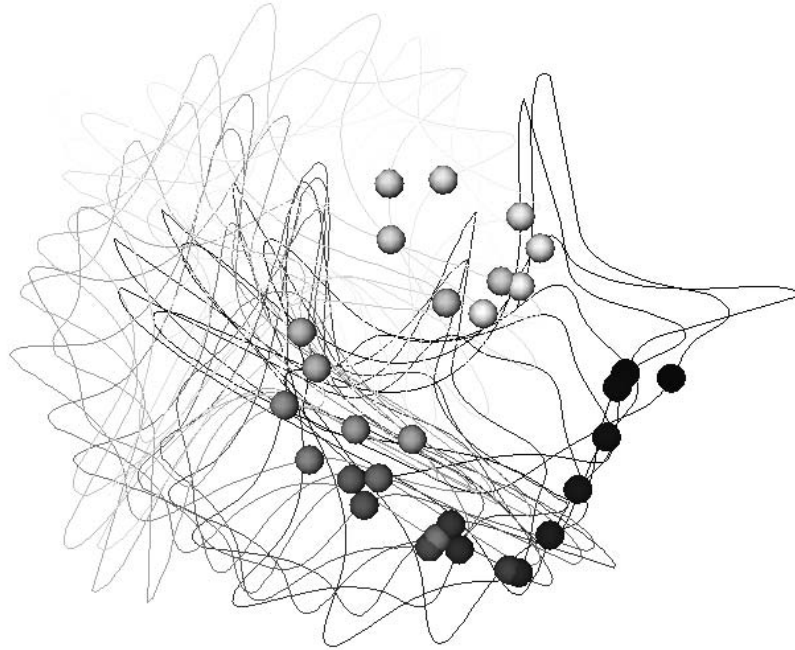


Fig. 7. A 2.3 s piece of the tip trajectory of a spiral wave in the 2D OGPV model under external forcing 1.2 mV/ms (0.24 nA/cell) duration 2 ms each, with period 110 ms. The balls show the tip positions at the beginning of each stimulus. Newer pieces are darker and older are lighter. This is defined by three processes stimulation+meander+ageing.

The resultant motion is a nonlinear interaction between the pattern of meander and the motion produced by the perturbations. The directed motion of resonant drift is much more robust if instead of choosing a fixed frequency, some kind of feed-back is used to synchronise the stimulation with the spiral wave rotation [29,30]. Such feedback control can provide the stable resonant drift in the OGPV model [31]. Figure 8 shows four tip trajectories produced by repetitive stimulation applied at four different fixed delays after the wavefront reached the bottom left corner. The delay determines the initial direction of drift. A repetitive perturbation of 15% the amplitude of the single shock defibrillation threshold produces a directed motion with a velocity of about 0.75 cm/s.

## 5.2 Defibrillation theory

The above results about resonant drift were for external perturbations measured relatively to the defibrillation threshold. This external influence was modelled as additional current in the equation for the transmembrane potential, with an explicit time dependence. However, this does not correspond to real situation, where the defibrillating voltage current is not applied across the membrane, but imposed extracellularly, and so the above results can be interpreted only in relative units to something that is also experimentally measurable, *e.g.* defibrillation threshold (DFT).

An absolute estimation of DFT can be obtained by quantitative theory of interaction of extracellular current with membrane excitation processes (see *e.g.* [32]) with theory of defibrillation [33,34]. This has been applied to the OGPV model in [37]. The basic idea of the description is that if the external current comes in through a part of the cell membrane in one direction, exactly the same current must come out through another part of the membrane. And the resulting model can be written in the form

$$\begin{aligned}
\partial_t V &= \frac{1}{2C} \left( f\left(V + \frac{I_{ext}(t)}{2\alpha}, \mathbf{u}_+, \mathbf{w}\right) + f\left(V - \frac{I_{ext}(t)}{2\alpha}, \mathbf{u}_-, \mathbf{w}\right) \right) + D\nabla^2 V \\
\partial_t \mathbf{u}_\pm &= \mathbf{g}\left(V \pm \frac{I_{ext}(t)}{2\alpha}, \mathbf{u}_\pm, \mathbf{w}\right) \\
\partial_t \mathbf{w} &= \mathbf{h}\left(V, \frac{\mathbf{u}_+ + \mathbf{u}_-}{2}, \mathbf{w}\right),
\end{aligned} \tag{4}$$

where the notations are mainly the same as in (1), (2), with the difference that  $V$  and  $\mathbf{w}$  are average values over the cell,  $I_{ext}$  external current flowing through the cell,  $\alpha$  effective cell conductivity with respect to this current (so that  $\pm I_{ext}/(2\alpha)$  is additional transmembrane voltage produced by this current), and  $\mathbf{u}_\pm$  are two vectors of faster gating variables, which behave significantly

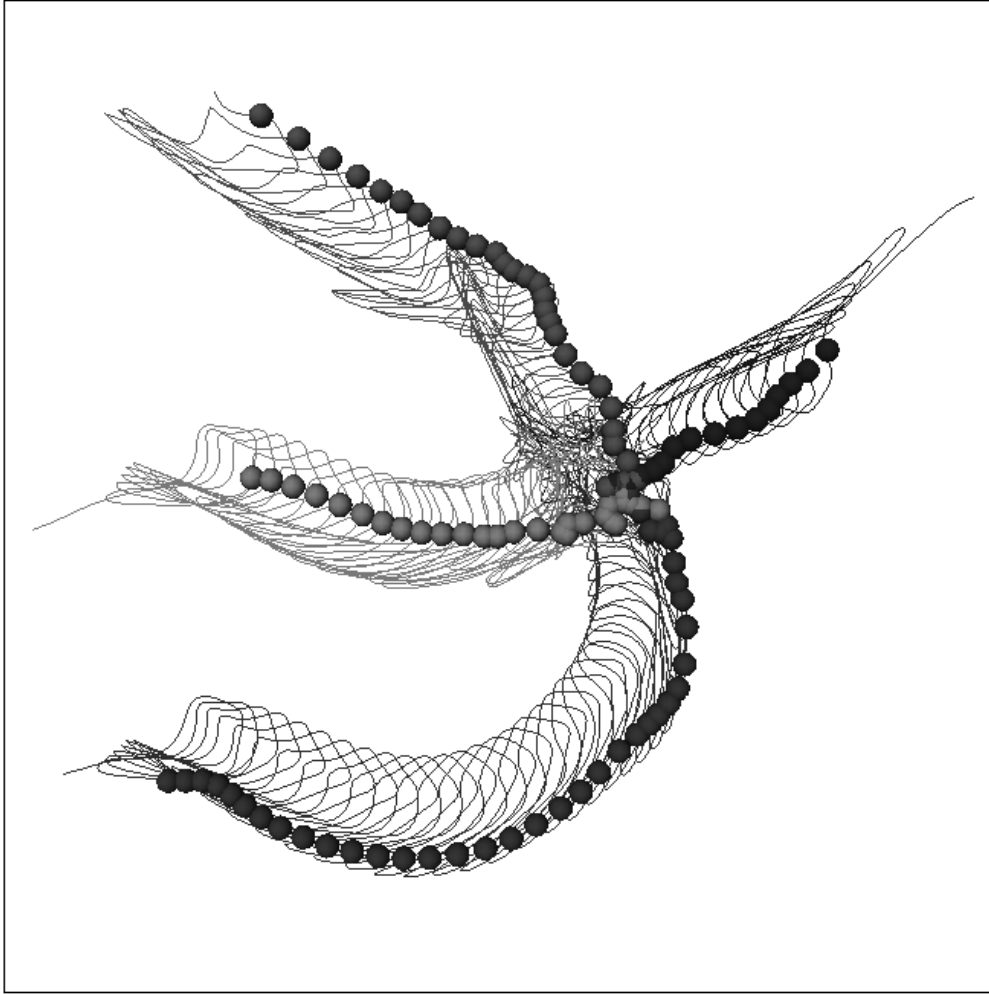


Fig. 8. Tips trajectories of resonantly drifting spirals, with feedback via registered electrode in the bottom left hand corner of the medium and delays 0, 25, 50 and 75 ms; average period of rotation is within 100 to 110 ms, square size 20 mm. The stimulations was by pulses 2 ms long 2 mV/ms (0.4 nA/cell) strong. The balls show the tip positions at the beginning of each stimulus. The visible fractures in the trajectories correspond to different phase locks between stimulation and meander.

different in the two membrane parts (these include ‘h’, ‘d’ and ‘f’). The gating variables ‘ $m_{\pm}$ ’ were not dynamic variables but fixed functions of the transmembrane voltages  $V \pm I_{ext}/(2\alpha)$ . All the dynamic quantities  $V$ ,  $I_{ext}$ ,  $\mathbf{u}_{\pm}$  and  $\mathbf{w}$  are functions of time and of the location of the cell in space;  $I_{ext}$  has been considered as a function of time only, *i.e.* it was assumed that the current is uniform over the tissue.

The validity of this simple system of equations depends on several assumptions, including the separation of time scale of various processes and approximation of the cell body by just two compartments; these were verified by

numerical tests in [37].

Typical responses of a spiral wave in this model to a 2 ms pulse of  $I_{ext}$  are shown on figs. 9 and 10. The stimulus has both depolarising and repolarising effects, and in the region ahead of the front the depolarisation effect overbalances the hyperpolarisation, and the front jumps forwards. The later evolution depends on how far the wavefront jumped. If the stimulus was above the threshold (see fig. 9, upper row), the front advances to the region where the tissue has not recovered yet, and the antegrade propagation is not possible. Hence, the front retracts, *i.e.* begins to collapse backwards, and the excited region shrinks until it vanishes, as the depolarising wavefront moves backwards and the repolarisation waveback carries on moving forwards.

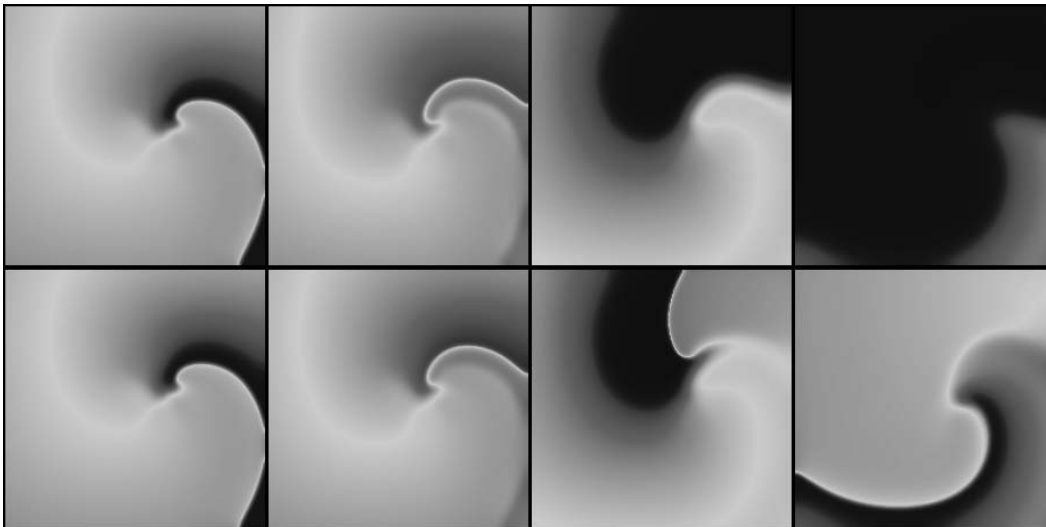


Fig. 9. Snapshots from movies of suprathreshold (above, with 800 nA/cell) and subthreshold (below, with 650 nA/cell) defibrillation by a spatially uniform 2 ms depolarising current pulse of a spiral wave shown on fig. 3. Time moments are chosen 0, 3, 40 and 80 ms (left to right) measured since the beginning of the stimulus.

A smaller (subthreshold) shock will produce a smaller advance in the position of the front and thus allow the possibility for it to recover its forward propagation. This possibility depends on two factors, the refractory state of the medium and the front curvature, which in turn depends on the geometry of the wavefront at the moment of the shock delivery. The lower row of fig. 9 shows the case when, after the shock, the propagation resumes not along the whole front, but only at the most concave segment of it, where the front curvature assist the propagation. This is sufficient to resume the rotation of the spiral wave. So, from this example it can be seen that DFT measured in two dimensions should be usually higher than that in one dimension.

We have applied the theory of [33] and [34] to calculate the one-dimensional DFT based on the properties of the single cell version of equations 4 and the restitution curve of original 1D model; this was found to be about 840 nA/cell.

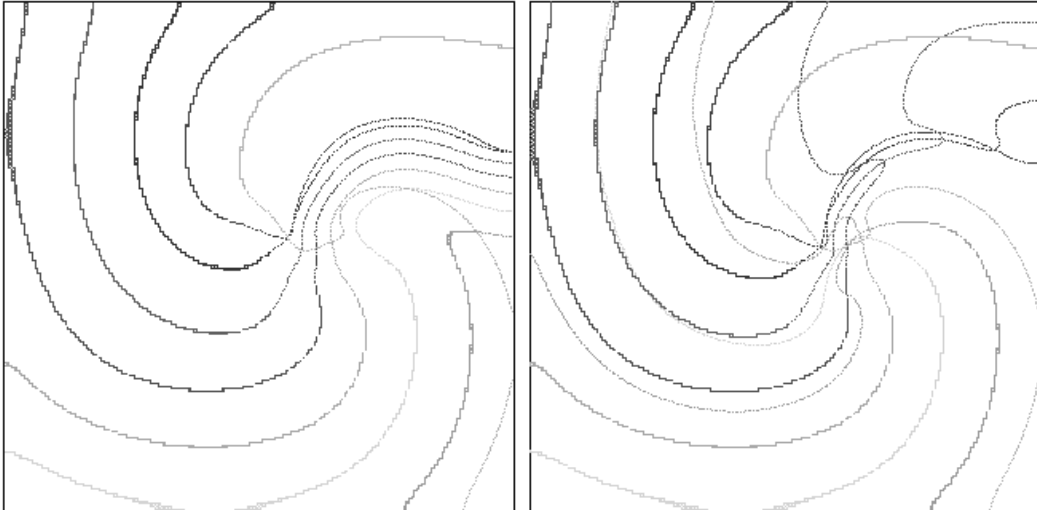


Fig. 10. Wavefronts and wavebacks visualised as  $-10$  mV isolines every 10 ms during (left) the suprathreshold and (right) subthreshold defibrillating shocks of Fig. 9. The first isoline is just before the defibrillating pulse was applied; the spiral wave is rotating counterclockwise.

The numerically computed 1D DFT was approx. 740 nA/cell, and in 2D, approx. 750 nA/cell. These values are for the rectangular current pulses of 2 ms duration, and with an intracellular conductivity assumed to give  $\alpha = 10\mu\text{S}$  (note that only the ratio of  $I_{ext}/\alpha$  is used in the model). This shows that the 2D effects are less important than other simplifications used. We believe that the crudest of the simplifications of that theory is the use of Fife technique [35], considering the excitation wave propagation as trigger waves in bistable media with one fast variable (the transmembrane voltage), while the conditions of propagation are governed by slow and local evolutions. The evolution in the OGPV model is more complicated, as there are three other variables  $\mathbf{u}$  of characteristic time scales roughly comparable to that of the transmembrane voltage.

## 6 Discussion

The results described above are all for homogeneous isotropic 2D models; the real ventricle is three-dimensional, with an anisotropic fibre architecture, and inhomogeneous, both in the sense of presence of inexcitable obstacles (such as blood vessels) that can act to pin reentrant sources [38], and with gradients in excitation properties, the transmural endo-to-epicardial differences described by Antzelevitch [15,16] and the base-to-apex differences that normally give the ventricular depolarisation and repolarisation the same polarity in the ECG. These anisotropies and inhomogeneities may mask the simple behaviours described above; in particular, the transmural rotational anisotropy cannot be

be eliminated by a simple coordinate transformation.

In three-dimensional homogeneous media the generalisation of a spiral wave is a scroll wave, that can have an open linear or curved filament, or a closed filament that (in principal [39], but almost certainly not in the heart) can be knotted. Instead of considering motion of the spiral tip, we need to consider filament motion. The asymptotical approaches to the dynamics of the scroll filaments have been proposed [40,41]; up to now only for non-meandering scrolls. Another approach to spiral and scroll waves motions comes from the application of the symmetries of the Euclidean Group of transformations [42]; but this still has to be developed to account for curved scroll wave dynamics.

It is interesting that some important properties of scroll waves, for instance, the filament tension [41], that determines the stability of the scroll filament shape, can be found from 2D simulation, and so it is computationally feasible to approach this using the OGPV model. Practical interest in this quantity is that if the tension is negative, then in thick enough medium, the scroll waves will tend to multiply, and this might provides yet another theoretical scheme for the development of fibrillation.

A striking feature about the anatomical organisation of the ventricular muscle is spiral organisation of the orientation of the muscle fibres on the epicardial surface. At any one point on the ventricular wall, as one penetrates the wall, the fibre orientation changes; there is a transmural rotational anisotropy. This rotational anisotropy not only may contribute to the formation of a re-entrant scroll wave [43], but can lead to spiral wave breakdown of a scroll wabe [44]. This provides a resolution to the paradox that numerical solutions, and experimental observations on thin ventricular slice preparations [45] demonstrate stable spiral while ventricular fibrillation is believed to be due to breakdown of spirals.

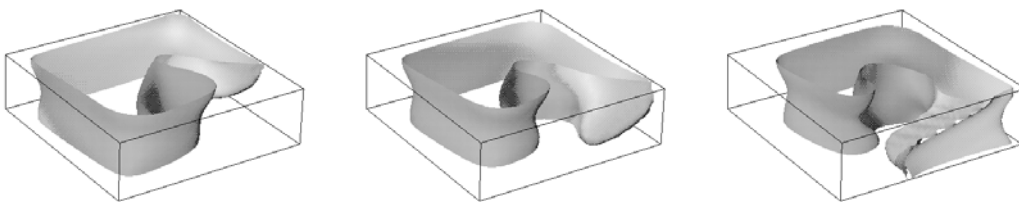


Fig. 11. Spiral wave in the OGPV model in thee dimensions with rotational anisotropy of 3:1 velocity ratio and total rotation angle  $120^\circ$ , size of preparation  $5 \times 5 \times 1.5$  mm.

Reproducing propagation in three-dimensional, biophysically realistic cardiac wall models with rotational anisotropy is possible — see Fig. 11, but a systematic investigation is in practice at the limits of available computing resources. Our preliminary approach is to use restructurable grid schemes for solving the full biophysical equations, with computations guided by phenomenology

known from simpler FitzHugh-Nagumo like caricatures. Within such a three dimensional model it is possible, in principle, to incorporate transmural gradients in the parameters of the excitation equations, with little increase in computational load. Although we can simulate the transmural shape changes in ventricular action potentials by scaling  $I_{to}$  [18], the actual changes in ionic currents with position in the ventricle is still being investigated, and so detailed simulations are perhaps premature. What is feasible is preliminary computations that simulate rather than reconstruct the changes in action potential shape, to see if these changes in action potential shape, and their rate dependence, have significant effects on propagation. Thus we are in a position to move into three-dimensional computations of propagation in currently realistic models of ventricular tissue, that include biophysical, anatomical and histological detail. The modelling of propagation phenomena in ventricular tissue and the whole ventricles is feasible. The real test of these computational investigations will be when they are validated against three dimensional visualisations of propagating activity in real hearts, obtained via laser-mapping and multiple electrode recordings.

## **Acknowledgement**

This work was partly funded by a Collaborative Biomedical Research Fellowship from The Wellcome Trust (045192) and grants from the Russian Fund for Basic Research (96-01-00592), EPSRC (GR/K/49775) and the Wellcome Trust (044365)

## References

- [1] A.L. Wit and M.J. Janse, *The ventricular arrhythmias of ischaemia and infarction* (Futura Pub Co, Mount Kisco, NY, 1993)
- [2] N. ElSherif, in *Cardiac Electrophysiology - from cell to Bedside*, edited by D.P. Zipes and J. Jalife (W.B. Saunders & Co, Philadelphia 1995)
- [3] R.S. Damle, N.M. Kanaan, N.S. Robinson, Y.Z. Ge, J.J. Goldberger and A.H. Kadish, *Circulation* **86**, 1547 (1992)
- [4] R.H. Clayton, A. Murray and R.W.F. Campbell, *J. Cardiovasc. Electrophysiol.* **6**, 616 (1995)
- [5] J.M. Davidenko, P.F. Kent and J. Jalife, *Physica D* **49**, 182 (1993)
- [6] A.L. Wit, M.A. Allesie, F.I.M. Bonke, W. Lammers, J. Smeets and J.J. Fenoglio, *Am. J. Cardiology* **49**, 166 (1982)
- [7] S.D. Girouard, J.M. Pastore, K.R. Laurita, K.W. Gregory and D.S. Rosenbaum, *Circulation* **93**, 603 (1996)
- [8] G. Beeler and H. Reuter, *J. Physiol. (Lond)* **268**, 963 (1989)
- [9] D. Noble *Oxsoft HEART Version 3.8 manual* (Oxsoft, Oxford, 1990)
- [10] D. Noble, S.J. Noble, G.C.L. Bett, Y.E. Earm, W.K. Ho and I.K. So, *Ann. N.Y. Acad. Sci.* **639**, 334 (1991)
- [11] C. Nordin, *Am. J. Physiol.* **265**, H2117 (1993)
- [12] C.H. Luo and Y. Rudy, *Circ. Res.* **74**, 1071-1097 (1993)
- [13] J.L. Zeng, K.R. Laurita, D.S. Rosenbaum and Y. Rudy, *Circ. Res.* **77**, 140 (1995)
- [14] D. Noble, *Chaos Solitons and Fractals* **5**, 321 (1995)
- [15] C. Antzelevitch, S. Sicouri, S.H. Litovsky, A. Lukas S.C. Krishnan J.M. DiDiego, G.A. Gintant and D.W. Liu, *Circ. Res.* **69**, 1427 (1991)
- [16] C. Antzelevitch, S. Sicouri, A. Lucas, V.V. Nesterenko, D.W. Liu and J.M. DiDiego, in *Cardiac Electrophysiology - from Cell to Bedside*, edited by D.P. Zipes and J. Jalife (W.B. Saunders & Co, Philadelphia, 1995)
- [17] V.N. Biktashev and A.V. Holden, *European Heart J.* **17**, Abstract Supplement: 597 (1996)
- [18] M.R. Boyett, A. Clough, A.V. Holden and J. Hyde, in *Computational Biology of the Heart*, edited by A.V. Panfilov and A.V. Holden (John Wiley, Chichester, 1997)

- [19] M.L. Presser, P.N. Münster and X. Huang,  
in *Cardiac Electrophysiology - from cell to Bedside*, edited by D.P. Zipes and  
J. Jalife (W.B. Saunders & Co, Philadelphia, 1995)
- [20] D.W. Frazier, P.D. Wolf, J.M. Wharton, A.S.L. Tang, W.M. Smith and  
R.E. Ideker, *J. Clin. Invest.* **83**, 1039 (1989)
- [21] C.F. Starmer, V.N. Biktashev, D.N. Romashko, M.R. Stepanov, O.N. Makarova  
and V.I. Krinsky *Biophys. J.* **65**, 1775 (1993)
- [22] I.R. Efimov, V.I. Krinsky and J. Jalife, *Chaos Solitons and Fractals* **5**, 513  
(1995)
- [23] M. Courtemanche and A.T. Winfree, *Int. J. Bifurcation and Chaos* **1**, 431 (1991)
- [24] V.A. Davydov, V.S. Zykov, A.S. Mikhailov and P.K. Brazhnik, *JETP Letters*  
**45**, 574 (1988)
- [25] V.N. Biktashev and A.V. Holden *Phys. Lett. A* **181**, 216 (1993)
- [26] V.S. Zykov, O.S. Steinbock and S.C. Müller, *Chaos* **4**, 509 (1994)
- [27] R.M. Mantel and D. Barkley, *Phys. Rev. E* **54**, 4791 (1996)
- [28] V.N. Biktashev, A.V. Holden and E.V. Nikolaev, *Int. J. Bifurcation and Chaos*  
**6**, 2433 (1996)
- [29] V.N. Biktashev and A.V. Holden, *J. Theor. Biol.* **169**, 101 (1994)
- [30] V.N. Biktashev and A.V. Holden, *Chaos Solitons and Fractals*, **5**, 575 (1995)
- [31] V.N. Biktashev and A.V. Holden, *Proc. Roy. Soc. London B* **263**, 1373 (1996)
- [32] W. Krassowska and J.C. Neu, *Biophys. J.* **66**, 1768 (1994)
- [33] A. Pumir and V. Krinsky, *Physica D* **91**, 205 (1996)
- [34] J.P. Keener, *J. Theor. Biol.* **178**, 313 (1996)
- [35] P.C. Fife, *J. Math. Anal. Appl.* **54**, 497 (1976)
- [36] V.N. Biktashev and A.V. Holden, *Proc. Roy. Soc. London B* **260**, 211 (1995)
- [37] V.N. Biktashev, A.V. Holden and H. Zhang, *Int. J. Bifurcation & Chaos*, **7**(2),  
1997, to appear
- [38] M. Vinson, A. Pertsov and J. Jalife, *Physica D* **72**, 119 (1994)
- [39] A.T. Winfree and S.H. Strogatz, *Physica D*, **8**, 35; **9**, 65, 333; **13**:221
- [40] J.P. Keener, "The dynamics of three dimensional scroll waves in excitable  
media"., *Physica D* **31**, 269 (1988)
- [41] V.N. Biktashev, A.V. Holden and H. Zhang, *Phil. Trans. Roy. Soc. London, ser  
A* **347**, 611 (1994)

- [42] A.V. Holden, *Nature* **397**:655 (1997)
- [43] A.V. Panfilov and J.P. Keener, *J. Cardiovasc. Electrophysiol.* **4**, 412 (1993)
- [44] A.V. Panfilov and J.P. Keener, *Physica D* **84**, 545 (1995)
- [45] J.M. Davidenko, A.M. Pertsov, R. Salomontsz, W. Baxter and J. Jalife, *Nature* **355**, 349 (1992)